Supplementary Material

A lightweight automatic workflow for expanding volcano-tectonic seismic catalogs: application to Villarrica Volcano, Chile

Sergio Morales[1,2], Sarah Jaye Oliva[3], and Andrés I. Ávila[4]

[1]Programa de Doctorado en Ingeniería, Universidad de La Frontera, Francisco Salazar 01145, Temuco 4811230, Chile
[2]Observatorio Volcanológico De los Andes del Sur (OVDAS), Servicio Nacional de Geología y Minería (SERNAGEOMIN), Rudecindo Ortega 03786, Temuco 4780000, Chile
[3]Department of Geophysics, Universidad de Chile, Santiago, Chile
[4]Departamento de Ingeniería Matemática, Universidad de La Frontera, Francisco Salazar 01145, Temuco 4811230, Chile

S1 Spatial distribution of unmatched events

The main text compares the locations of the 551 events matched between the two catalogs (Figure 5 of the main text). Here we extend that analysis to the events that did not match: the 209 VT events detected exclusively by OVDAS analysts (Only Manual) and the 695 events detected exclusively by the automatic workflow (Only Auto), whose spatial distributions are shown in Figures S1 and S2, respectively.

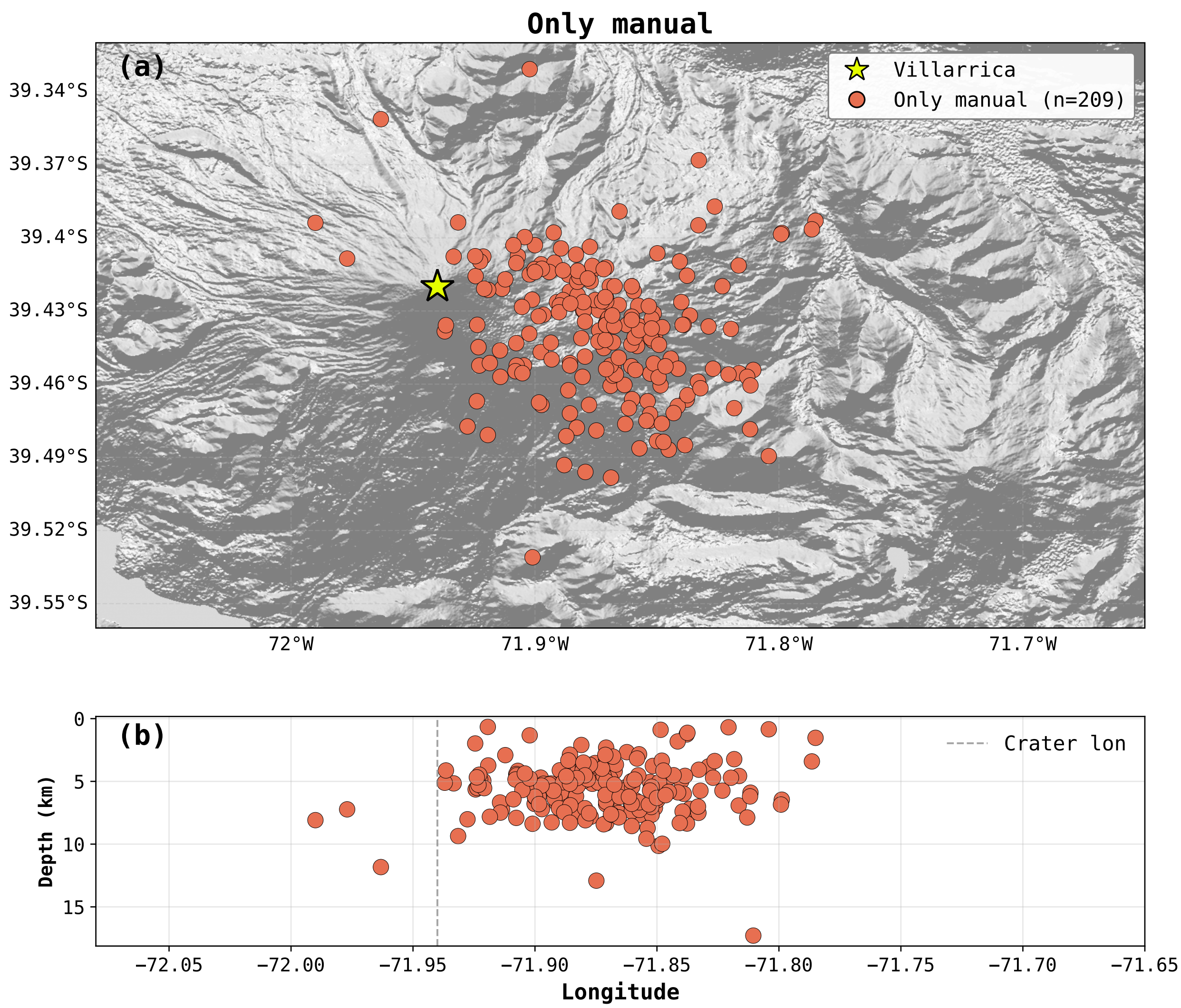

Figure S1: Spatial distribution of the 209 VT events detected exclusively by OVDAS analysts and not present in the automatic catalog. (a) Epicentral map overlaid on a hillshade relief model of the Villarrica region. The yellow star marks the volcano summit. (b) Longitude–depth cross-section of the same events. The dashed vertical line indicates the longitude of the summit crater.

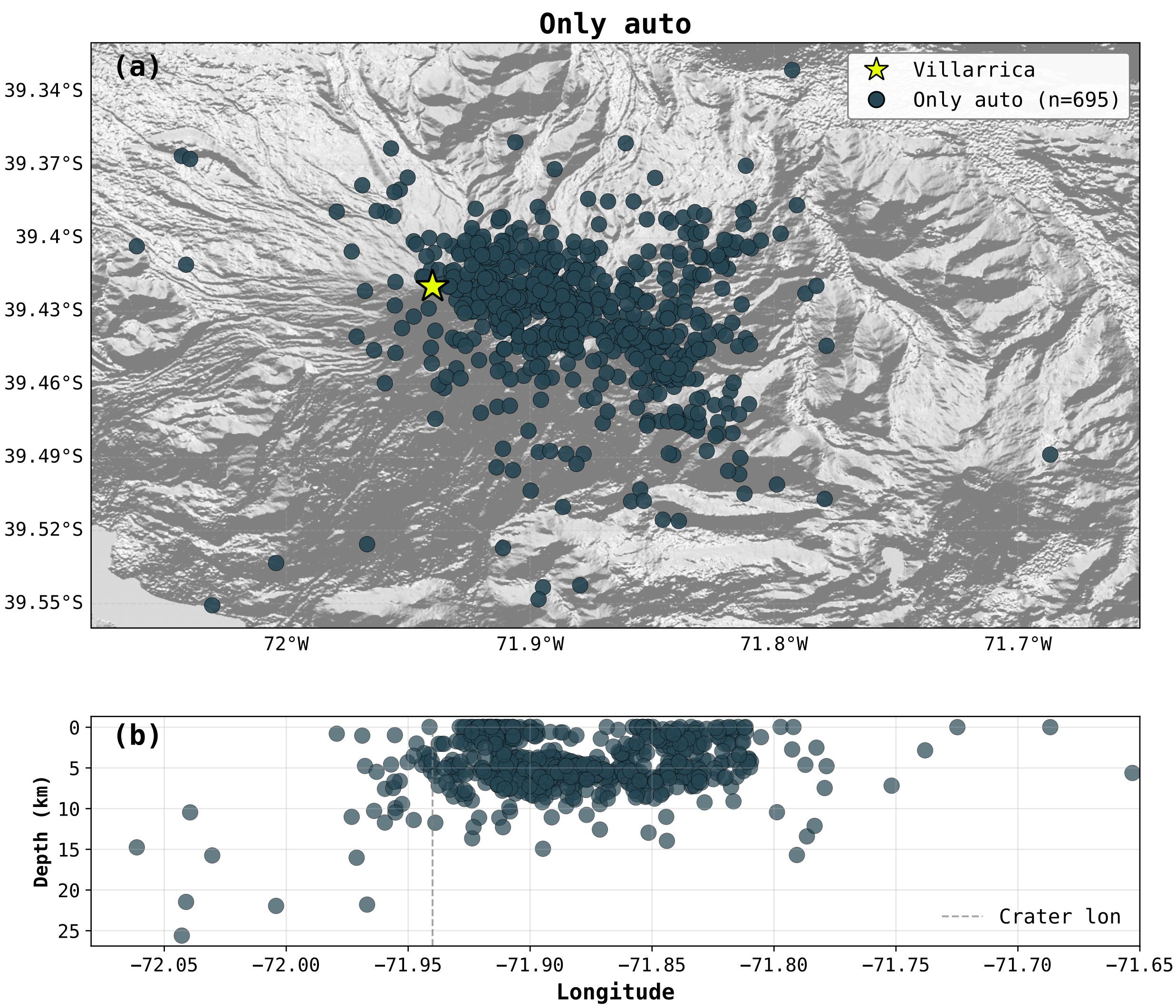

Figure S2: Spatial distribution of the 695 VT events detected exclusively by the automatic workflow and not present in the OVDAS analyst catalog. (a) Epicentral map overlaid on a hillshade relief model of the Villarrica region. The yellow star marks the volcano summit. (b) Longitude–depth cross-section of the same events. The dashed vertical line indicates the longitude of the summit crater.

S2 Individual location comparisons

Three representative matched events are examined individually in Figures S3–S5 to illustrate qualitatively distinct outcomes in the relationship between the NonLinLoc [1] and HYPO71 [2] location methods. In each figure, the upper panel shows the epicentral view and the lower panel shows the longitude–depth cross-section. The blue circle and red circle indicate the NonLinLoc (automatic) and HYPO71 (manual) epicenters, respectively, and the blue scatter cloud shows the NonLinLoc posterior probability density sampled solutions. Orange triangles indicate stations used by both methods, red triangles those used exclusively by HYPO71, and blue triangles those used exclusively by NonLinLoc. The dashed red ellipse indicates the HYPO71 horizontal uncertainty ($\pm 1\sigma$, ERH).

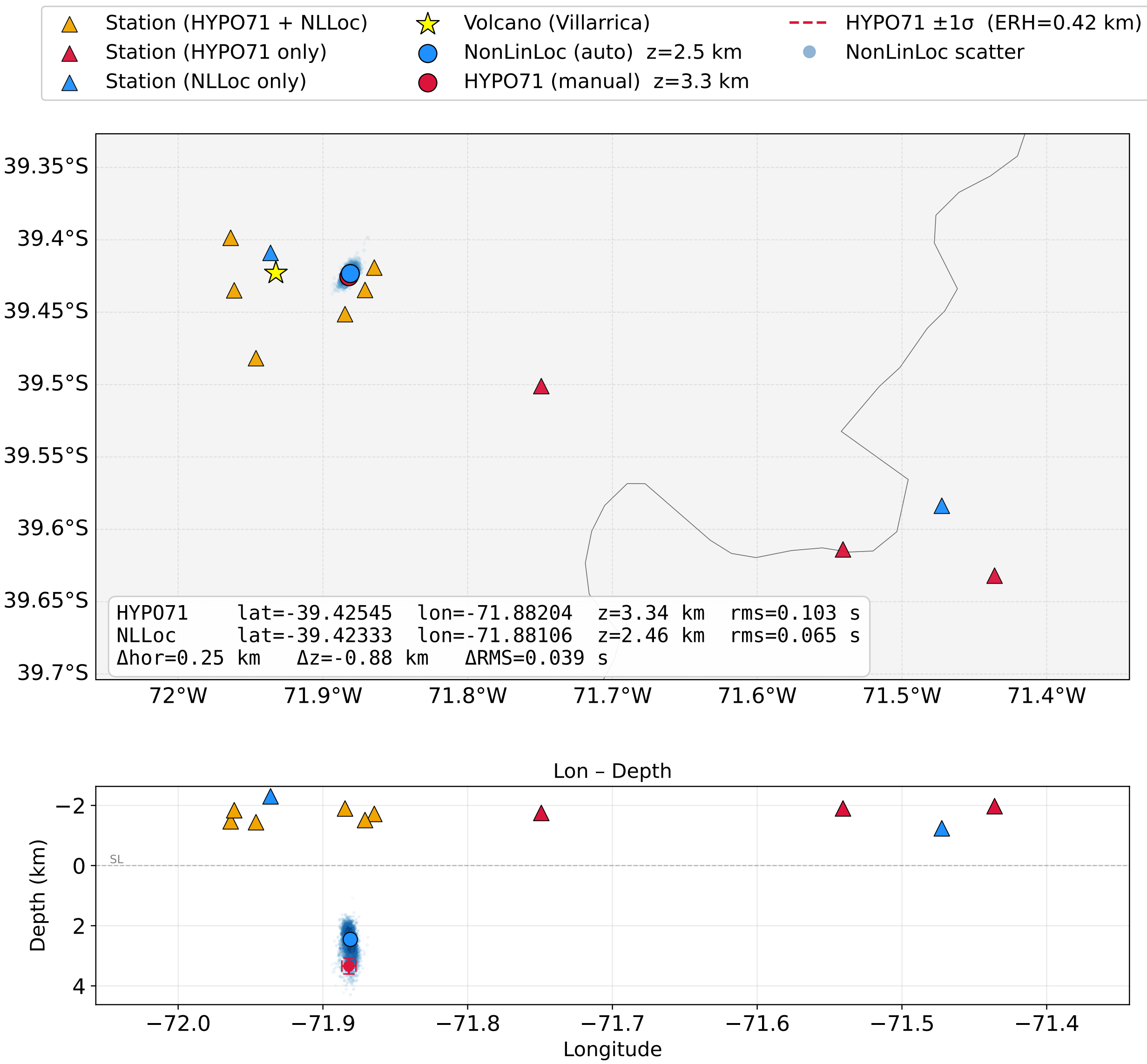

Figure S3: Well-constrained event in which both methods yield consistent solutions. Both hypocenters fall within the main lobe of the scatter cloud ($\Delta\mathrm{hor} = 0.25$ km, $\Delta z = 0.88$ km, $\Delta\mathrm{RMS} = 0.039$ s, $\mathrm{ERH} = 0.42$ km).

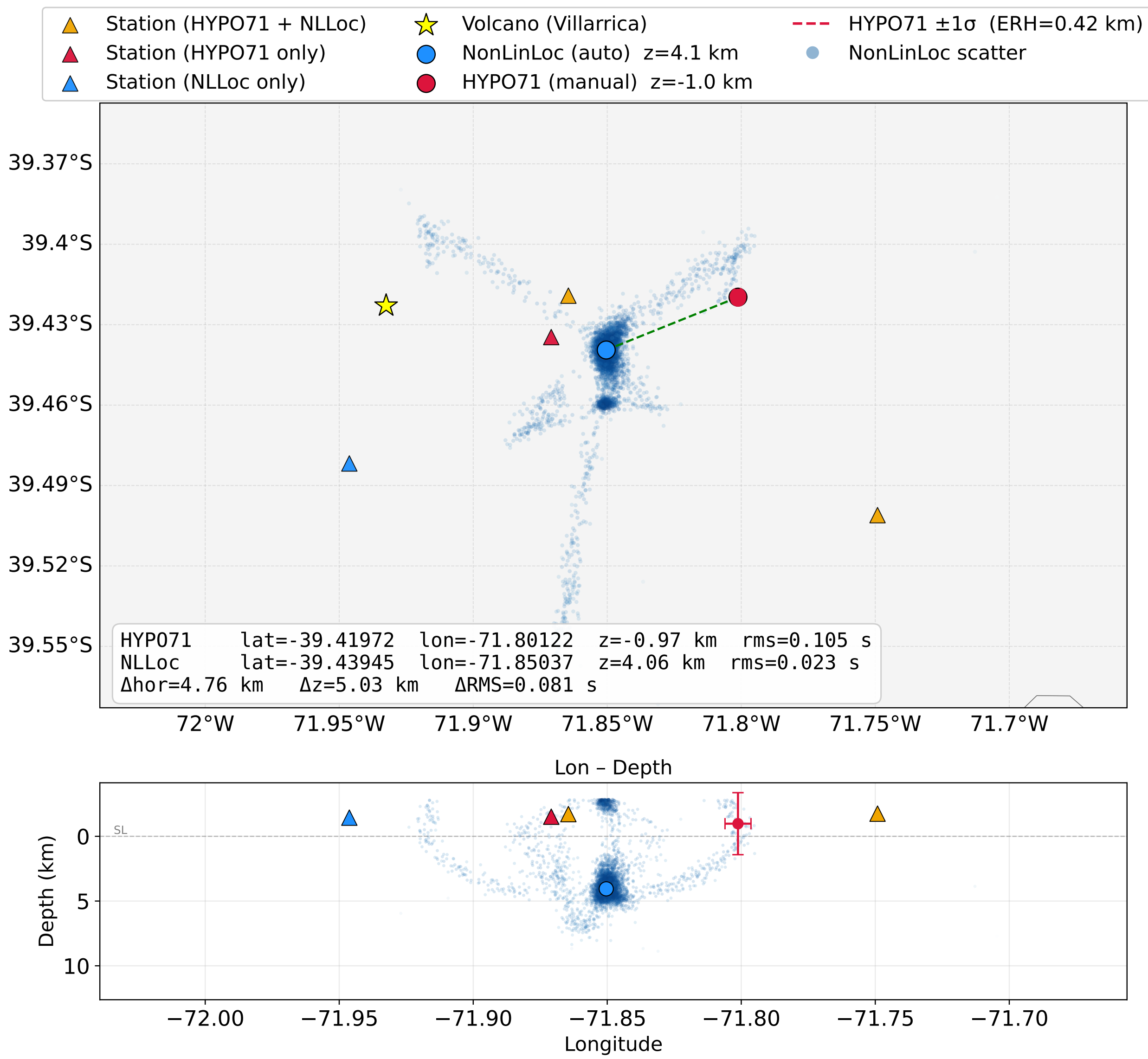

Figure S4: Event in which the HYPO71 solution lies outside the NonLinLoc posterior scatter cloud. The HYPO71 solution places the hypocenter at $z = -1.0$ km (above sea level) with RMS $= 0.105$ s, while the NonLinLoc solution converges to $z = 4.1$ km with RMS $= 0.023$ s and falls within the dense core of the scatter cloud. The elongated, cross-shaped scatter pattern reflects poor depth constraint imposed by the available station geometry, suggesting that the HYPO71 solution corresponds to a local minimum not representative of the true posterior (Δhor $= 4.76$ km, $\Delta z = 5.03$ km).

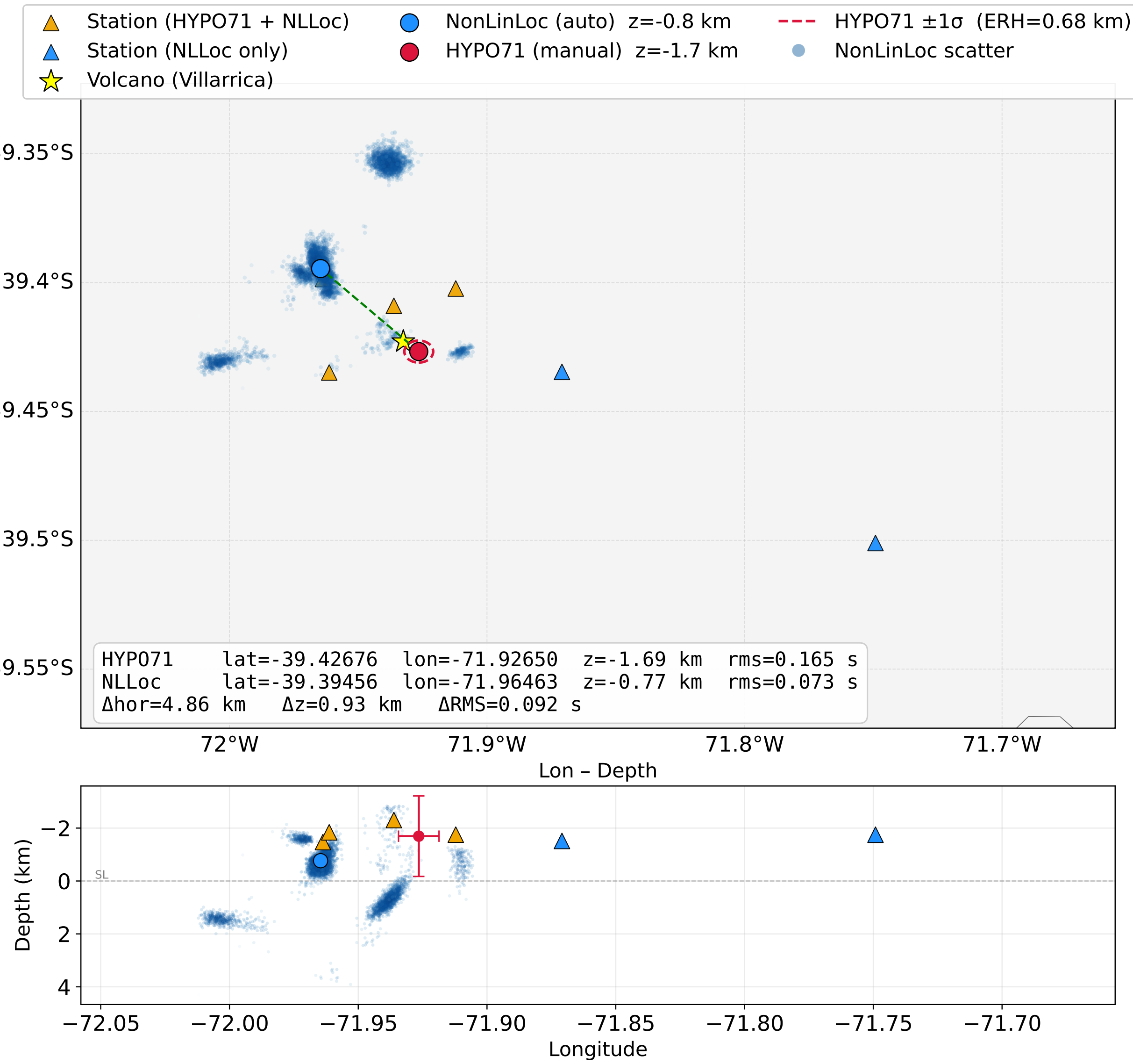

Figure S5: Event in which the HYPO71 manual solution lies outside the main lobes of the NonLinLoc posterior scatter cloud, falling instead in a diffuse, low-probability region of the distribution. The NonLinLoc solution ($z = -0.8$ km, RMS = 0.073 s) aligns with one of the primary modes of the scatter cloud, while the HYPO71 solution ($z = -1.7$ km, RMS = 0.165 s, ERH = 0.68 km) falls between them. Even accounting for the reported HYPO71 uncertainty, the horizontal offset (Δhor = 4.86 km) is substantially larger than the ERH, indicating that the discrepancy between methods reflects a genuine disagreement in source location rather than an artifact of location uncertainty alone.

References

[1] Lomax, A., Virieux, J., Volant, P., Berge-Thierry, C.: Probabilistic earthquake location in 3D and layered models: Introduction of a Metropolis-Gibbs method and comparison with linear locations. Advances in seismic event location, 101–134 (2000) https://doi.org/10.1007/978-94-015-9536-0$_5$

[2] Lee, W.H.K., Lahr, J.C., Valdes, C.M.: 85.17 The HYPO71 earthquake location program. In: International Geophysics vol. 81, pp. 1641–1642. Elsevier, Amsterdam (2003). https://doi.org/10.1016/S0074-6142(03)80296-6